Chinese Chemical Letters 32 (2021) 21–24

Contents lists available at ScienceDirect

Chinese Chemical Letters

journal homepage: www.elsevier.com/locate/cclet

Communication

In-situ electro-deposition synthesis of MnO_x-$NiCo_2O_4$ monolithic catalyst with rich phase interfaces

Dongdong Wang[a,b], Yingchao Du[a,b], Xiaoze Wang[a,b], Zhaxi Cuo[a,c,*], Yunfa Chen[a,b,d,*]

[a] *State Key Laboratory of Multi-Phase Complex Systems, Institute of Process Engineering, Chinese Academy of Sciences, Beijing 100190, China*
[b] *University of Chinese Academy of Sciences, Beijing 100049, China*
[c] *Key Laboratory of Resource Chemistry and Ecoenviromental Protection in Tibetan Plateau, (Qinghai Nationalities University), State Ethnic Affairs Commission, School of Chemistry and Chemical Engineering, Xining 810007, China*
[d] *CAS Center for Excellence in Urban Atmospheric Environment, Xiamen 361021, China*

ARTICLE INFO

Article history:
Received 30 September 2020
Received in revised form 30 October 2020
Accepted 4 November 2020
Available online 5 November 2020

Keywords:
Rich phase interfaces
In-situ electro-deposition
Active oxygen species
Benzene combustion
MnO_x-$NiCo_2O_4$

ABSTRACT

A hierarchically structured MnO_x-$NiCo_2O_4$ monolithic catalyst with rich phase interfaces was designed by a simple, eco-friendly and time-saving *in-situ* electro-deposition method. The abundance of active oxygen species due to this rich phase interfaces contributed to the excellent benzene combustion performance of MnO_x-$NiCo_2O_4$-2:2 sample, oxidizing about 90% of benzene (T_{90}) at 198 °C under 12000 h^{-1} gaseous hourly space velocity. This work shed new light on the design of excellent monolithic catalysts, which might pave the way for the industrialization of benzene combustion.

In order to remove industrial volatile organic compounds (VOCs) more effectively, economically and practically, it is undergoing a transformation from traditional powder catalysts to monolithic catalysts with lower pressure drop and lower active phase loading mass [1–4]. Aiming at increasing the activity and service life of monolithic catalysts by generating a stronger interphase anchorage force between the active phase and the support, it is an inevitable trend that *in-situ* growth strategy will replace the indirect synthesis strategy of combining the powder catalyst with support by coating or impregnating [4–6]. However, there is still no significant progress in industrial application of monolithic catalysts, which is mainly due to the non-universal *in-situ* synthesis strategy to limit the diversity of monolithic catalysts. Electro-deposition is a relatively inexpensive and rapid inorganic solid-state synthesis method that allows the deposition of metal layers on conductive substrates with complex structures. The salient features of electro-deposition are mainly reflected in the following aspects: electro-deposition process can be performed near room temperature from water-based electrolytes; regulation of product component can be realized by changing the electrolyte ratio or performing multistep electro-deposition; products can be scaled down to the deposition of a few atoms or up to large dimensions; kinetic parameters can be easily regulated by changing current density and thermodynamic parameters can be easily regulated by changing electrode potential [7,8]. Therefore, *in-situ* electro-deposition strategy might shed new light on the enrichment of monolithic catalysts variety for the complete removal of VOCs.

The importance of active oxygen species, which are directly involved in VOCs combustion reactions, has been well demonstrated in previous work [9]. At present, the widely used methods to enhance active oxygen species are to create intrinsic defects by regulating synthesis process or introducing doping elements. In fact, phase interfaces with higher energy states often produce abundant defects that can also induce a significant number of active oxygen species nearby [10]. Therefore, it is an effective and feasible way to produce active oxygen species by preparing multiphase structure materials with abundant phase interfaces.

Herein, a series of MnO_x-$NiCo_2O_4$ monolithic catalysts with rich phase interfaces were designed and synthesized by a two-step *in-situ* electro-deposition method. The special multistage structure, lamellar nickel-cobalt spinel phase grows vertically on the surface of manganese oxide which uniformly coated three-dimensional nickel foam skeleton, ensures the formation and full exposure of

* Corresponding authors at: State Key Laboratory of Multi-Phase Complex Systems, Institute of Process Engineering, Chinese Academy of Sciences, Beijing 100190, China.
E-mail addresses: zhaxicuo@ipe.ac.cn (Z. Cuo), chenyf@ipe.ac.cn (Y. Chen).

https://doi.org/10.1016/j.cclet.2020.11.012
1001-8417/

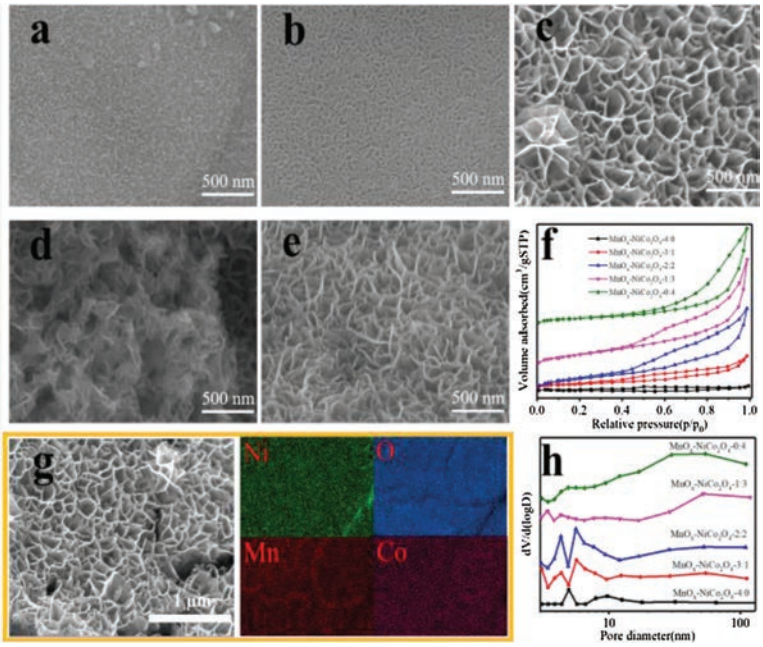

Fig. 1. SEM images of (a) MnO_x-$NiCo_2O_4$-4:0, (b) MnO_x-$NiCo_2O_4$-3:1, (c) MnO_x-$NiCo_2O_4$-2:2, (d) MnO_x-$NiCo_2O_4$-1:3 and (e) MnO_x-$NiCo_2O_4$-0:4. (g) Element distribution of MnO_x-$NiCo_2O_4$-2:2 sample. (f) N_2 adsorption-desorption isotherm and (h) pore size distribution of these monolithic catalysts, respectively.

the phase interface. As expected, MnO_x-$NiCo_2O_4$-2:2 monolithic catalyst reported in this work can completely transform 90% benzene at 198 °C under 12000 h^{-1} gaseous hourly space velocity.

In the three-electrode system of this experiment, nickel foam was directly selected as the working electrode, and counter electrode and reference electrode were platinum sheet and saturated calomel electrode (SCE), respectively. The electro-deposition process lasts two minutes and involves two successive steps: anodic electro-deposition with manganese acetate as electrolyte and cathode electro-deposition with cobalt nitrate and nickel nitrate mixture ($Co(NO_3)_2$:$Ni(NO_3)_2$ = 2:1) as electrolyte. The loading ratio of manganese oxide and nickel-cobalt spinel was adjusted by changing the reaction time of the two electro-deposition steps, a series of catalysts were thus synthesized and named as MnO_x-$NiCo_2O_4$-m:4-m (m = 0, 1, 2, 3, 4). At last, all samples were calcined at 573 K for 4 h.

The powder X-ray diffraction (XRD) data used to define the catalyst phase were obtained by Panalytical X'Pert PRO MPD. Scanning electron microscopy (SEM, JEOL JSM-6700 F) with an energy dispersive X-ray (EDX) spectroscopy can not only analyze the microscopic morphology of the catalysts, but also calculate the loading ratio of manganese oxide and nickel cobalt spinel phases in different samples. The specific surface area and pore size distribution of the monolithic catalysts were analyzed on the Quantachrome NOVA 3200e equipment by using Brunauer-Emmett-Teller (BET) and Barrett-Joyner-Halenda (BJH) methods, respectively. Raman spectra of all catalysts were collected by Renishaw inVia-Reflex Raman Spectrometer. To evaluate the redox activity of the monolithic catalysts, H_2 temperature-programmed-reduction (H_2-TPR) tests were performed on Quantachrome chemBET pulsar TPR/TPD chemisorption analyzer. The details of catalysts evaluation are in Supporting information.

Figs. 1a-e show the microscopic morphology of the catalysts, and the huge difference in morphology between these samples indicates that the loading ratio of manganese oxide and nickel-cobalt spinel does affect the structure of monolithic catalysts. The monolithic catalyst of single manganese oxide (Fig. 1a) shows crisscrossing small worm-like projections, however, the monolithic catalyst of single nickel-cobalt spinel (Fig. 1e) appears an irregular grid structure constructed by a series of nearly perpendicularly oriented lamellae, which greatly expands its specific surface area and gas channel. Hence, in the specific surface area and pore size distribution results shown in Figs. 1f and h and Table 1, single nickel-cobalt spinel sample possesses larger hysteresis area and wider pore size distribution than single manganese oxide sample. As shown in Fig. 1b, MnO_x-$NiCo_2O_4$-3:1 inherits the small particle size of manganese oxide and the growth orientation of nickel-cobalt spinel, exhibits a vertically oriented

Table 1
Active phase loading ratio, physical characterization and catalytic performance of as-prepared samples.

Sample	Loading ratio (%)	BET surface area (m^2/g)	Pore size (nm)	Active phase BET surface area [a] (m^2/g)	T_{50} (°C)	T_{90} (°C)
MnO_x-$NiCo_2O_4$-4:0	5.0	1.66	3.48	12.3	197	244
MnO_x-$NiCo_2O_4$-3:1	4.9	4.49	7.36	70.3	204	>250
MnO_x-$NiCo_2O_4$-2:2	4.8	10.72	7.62	201.5	176	198
MnO_x-$NiCo_2O_4$-1:3	5.1	10.45	9.99	184.4	200	223
MnO_x-$NiCo_2O_4$-0:4	5.0	6.71	13.83	113.3	183	244

[a]Active phase BET surface area was calculated by the following equation: Active phase BET surface area $= \frac{\text{BET surface area} - (1 - \text{Loading ratio}) \times \text{nickel foam BET surface area}}{\text{Loading ratio}}$, and nickel foam BET surface area was 1.1 m^2/g.

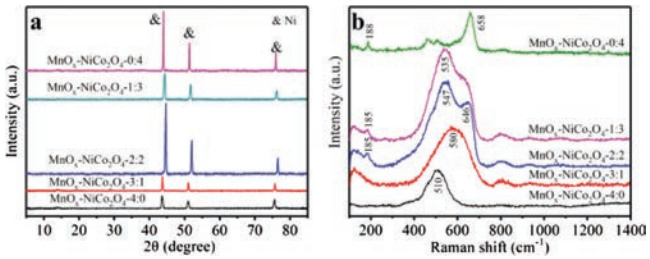

Fig. 2. (a) XRD patterns and (b) Raman spectra of all these samples.

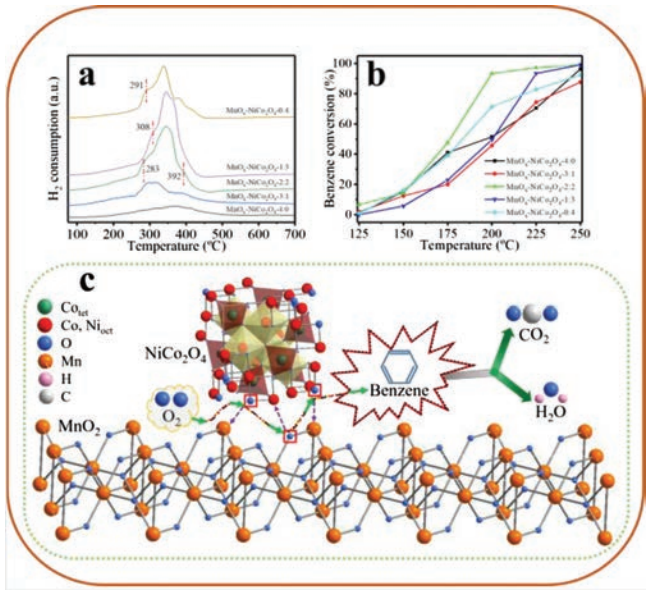

Fig. 3. (a) H_2-TPR patterns, (b) benzene conversions over prepared catalysts at 12,000 h^{-1}. (c) Schematic diagram of reaction mechanism.

lamellar structure with inadequate growth and dense distribution, and its specific surface area has been improved to some extent. For MnO_x-$NiCo_2O_4$-2:2 sample (Fig. 1c), lamellae are well developed in vertical direction and the spaces between the lamellae are abundant. Naturally, it has the largest specific surface area and the widest pore distribution of these monolithic catalysts, moreover, its specific surface area of the active phase component is up to 201.5 m^2/g. According to Fig. 1d, the growth direction of MnO_x-$NiCo_2O_4$-1:3 sample is chaotic, which is manifested as three-dimensional disordered stacking of lamellae structures. The SEM element distribution mapping of MnO_x-$NiCo_2O_4$-2:2 sample is shown in Fig. 1g, the uniform distribution of the four elements indicates that nickel-cobalt spinel grows indiscriminatingly on the surface of manganese oxide. In order to evaluate the actual element mole ratios of these multi-stage catalysts, ICP results were shown in Table S1 (Supporting information). The actual ratio of manganese and cobalt is basically the same as the theoretical value, while the higher nickel content may be due to the partial stripping of the carrier (nickel foam).

The XRD patterns of these monolithic catalysts were shown in Fig. 2. Unfortunately, due to the extremely low loading of the active phase (5% ± 0.2%), only the diffraction peaks of nickel foam were detected in the XRD patterns. According to the previous report (PDF 01−070-0989), diffraction peaks at 44.6°, 52.0° and 76.6° can be attributed to (111), (200) and (220) crystal faces of metallic nickel, respectively [11]. Raman spectrum is also a powerful tool for determining the phase structure on the premise of defining elements, especially some metallic oxides with low crystallinity, therefore, Raman spectra of these monolithic catalysts were detected and shown in Fig. 2 [12–14]. The characteristic peaks of spinel structures were detected in single nickel-cobalt spinel sample, 658 cm^{-1} peak can be attributed to cobalt-oxygen bond vibrations at octahedron sites (CoO_6) and 188 cm^{-1} peak can be attributed to cobalt-oxygen bond vibrations at tetrahedron sites (CoO_4) [15]. The monolithic catalyst of single manganese oxide shows unique characteristic peak at 510 cm^{-1}, which is the deformation modes of Mn-O-Mn chains in the MnO_2 phase [16]. For MnO_x-$NiCo_2O_4$-3:1 catalyst, a wide peak which can be attributed to the stretching vibration of Mn-O bond appeared at 580 cm^{-1}, and no characteristic peak of nickel-cobalt spinel was detected, which indicated that its growth was not sufficient, which was consistent with SEM results [17,18]. Of course, both manganese oxide and nickel-cobalt spinel characteristic peaks were detected in MnO_x-$NiCo_2O_4$-2:2 and MnO_x-$NiCo_2O_4$-1:3 samples. It is worth mentioning that the nickel-cobalt spinel characteristic peak of MnO_x-$NiCo_2O_4$-2:2 catalyst has an obvious red shift, indicating that the cobalt-oxygen bond weakens, which is very conducive to the transformation of cobalt ions between bivalent and trivalent, thus accelerating the catalytic oxidation process.

Fig. 3a exhibits the H_2-TPR patterns of these monolithic catalysts, which may clarify the role of manganese oxide and nickel-cobalt spinel loading ratio for catalysts reducibility. The oxidation of hydrogen continued in single manganese oxide monolithic catalyst over a wide temperature range, which reflects a low crystallinity and/or rich defects characteristic of MnO_x active phase. However, single nickel-cobalt spinel monolithic catalyst has two characteristic peaks with an area ratio of approximately 1:3, which also conforms to the reduction process of spinel material, namely the phase transition from $NiCo_2O_4$ to $NiCoO_2$, and from $NiCoO_2$ to metal phase respectively [19]. It is worth mentioning that MnO_x-$NiCo_2O_4$-2:2 sample shows the first characteristic peak at the lowest temperature of 283 °C, which can be attributed to the proper ratio of manganese oxide and nickel-cobalt spinel phase resulting in a rich phase interface. In Fig. 3b, 100 ppm benzene was selected to evaluate the VOCs removal capability of the monolithic catalyst at a gaseous hourly space velocity (GHSV) of 12,000 h^{-1}. The benzene catalytic activity of the prepared catalysts is basically consistent with H_2-TPR reducibility. MnO_x-$NiCo_2O_4$-2:2 sample completely catalyzed 50% and 90% of benzene to H_2O and CO_2 at 176 °C and 198 °C, respectively. As can be seen from Fig. S2 (Supporting information), MnO_x-$NiCo_2O_4$-2:2 sample possesses excellent long-term stability, degradation ratio of benzene was still as high as 95% after 48 h test. The carbon balance of all the samples was greater than 96% during the reaction above T_{90} temperature, indicating that the by-products could be ignored. A detailed analysis of the reactivity sequence of MnO_x-$NiCo_2O_4$ catalysts for T_{10}, T_{50} and T_{90} were exhibited in Supporting information. Furthermore, we have calculated the reaction rate of each sample at 150 °C (benzene conversion of all the samples is between 5%–20%), 198 °C (T_{90} of MnO_x-$NiCo_2O_4$-2:2 sample) and drawn the Arrhenius plots for the oxidation of benzene over these catalysts, all these results were presented in Table S1 and Fig. 1. In combination with the structural analysis and catalytic performance results, a schematic diagram of benzene reaction mechanism with the participation of MnO_x-$NiCo_2O_4$ monolithic catalyst is presented in Fig. 3c. It is well known that active oxygen species play an important role in thermocatalytic VOCs removal, and its content directly affects the reaction rate of benzene combustion [9,20]. In addition, compared with bulk phase, the phase interface

is often in a higher energy state due to abundant structural defects and interphase forces, thus generating active oxygen species with a higher probability. In order to deepening the understanding and demonstration of these defects, X-ray photoelectron spectra (XPS) and electron paramagnetic resonance (EPR) was tested and shown in Figs. S3 and S4 (Supporting information). MnO_x-$NiCo_2O_4$-2:2 sample indeed possesses a symmetrical peak at g = 2.01, however, other samples cannot detect this characteristic peak of oxygen radical, so it indicated that the rich phase interfaces can escalatory oxygen vacancies. Therefore, benzene combustion reaction occurs mainly at the interface of manganese oxide and nickel-cobalt spinel, a complete redox cycle consists of the following two steps: lattice oxygen bonds at the phase interface form active oxygen species and leave oxygen vacancies, active oxygen species participate in benzene combustion reaction to produce carbon dioxide and water; oxygen molecules occupy the oxygen vacancies left, and the lattice oxygen at the phase interface is re-formed [21]. Hence, MnO_x-$NiCo_2O_4$-2:2 sample possesses lowest T_{90} of benzene combustion due to the presence of a vertically oriented spinel phase that allowed the phase interface to be fully exposed. This also explains the phenomenon that dense-growing MnO_x-$NiCo_2O_4$-3:1 sample and three-dimensional disorderly stacked MnO_x-$NiCo_2O_4$-1:3 sample exhibited lower benzene catalytic activity than the single-phase monolithic catalysts due to the lack of exposed phase interfaces.

In this work, a series of MnO_x-$NiCo_2O_4$ monolithic catalysts with great morphological differences have been prepared by using a two-step electro-deposition strategy and felicitously adjusting the loading ratio of manganese oxide and nickel-cobalt spinel. The manganese oxide phase uniformly covering the nickel foam surface and the nickel-cobalt spinel phase growing almost vertically resulted in an abundant phase interfaces of MnO_x-$NiCo_2O_4$-2:2 sample. This rich phase interface produced abundant active oxygen species which is essential for benzene combustion. Therefore, MnO_x-$NiCo_2O_4$-2:2 monolithic catalyst possesses an excellent catalytic activity, and completely oxidizing 90% of benzene at 198 °C under a gaseous hourly space velocity of 12000 h^{-1}. In conclusion, we have successfully prepared MnO_x-$NiCo_2O_4$-NF monolithic catalysts with abundant phase interfaces through a simple electro-deposition method, which not only provides a feasible path for designing materials by electro-deposition but also enriches the *in-situ* synthesis strategy of monolithic catalysts.

Declaration of competing interest

The authors report no declarations of interest.

Acknowledgments

This research described above was financially supported by National Key R&D Program of China (Nos. 2017YFC0211503, 2016YFC0207100), the National Natural Science Foundation of China (Nos. 21401200, 51672273) and the Open Research Fund of State Key Laboratory of Multi-phase Complex Systems (No. MPCS-2017-D-06).

Appendix A. Supplementary data

Supplementary material related to this article can be found, in the online version, at doi:https://doi.org/10.1016/j.cclet.2020.11.012.

References

[1] M. Waqas, P.M. Kouotou, A. El Kasmi, Y. Wang, Z.Y. Tian, Chin. Chem. Lett. 31 (2020) 1201–1206.
[2] Y. Ji, J. Xie, Y. Yang, et al., Chin. Chem. Lett. 31 (2020) 855–858.
[3] S. Zhao, B. Xu, L. Yu, Y. Fan, Chin. Chem. Lett. 29 (2018) 884–886.
[4] M. Zheng, D. Yu, L. Duan, W. Yu, L. Huang, Catal. Commun. 100 (2017) 187–190.
[5] B. Xiao, K. Zhao, L. Zhang, et al., Catal. Commun. 116 (2018) 1–4.
[6] D. Wang, Z. Cuo, S. Li, M. Zhang, Y. Chen, CrystEngComm 22 (2020) 2371–2379.
[7] G. Helen Annal Therese, P. Vishnu Kamath, Chem. Mater. 12 (2000) 1195–1204.
[8] Z. Wu, Y. Zhu, X. Ji, J. Mater. Chem. A 2 (2014) 14759–14772.
[9] C. He, J. Cheng, X. Zhang, et al., Chem. Rev. 119 (2019) 4471–4568.
[10] Z. Li, Q. Yan, Q. Jiang, et al., Appl. Catal. B 269 (2020)118827.
[11] G.W. Yang, C.L. Xu, H.L. Li, Chem. Commun. (2008) 6537–6539.
[12] C. Wang, X. Zou, H. Liu, et al., Appl. Surf. Sci. 486 (2019) 420–430.
[13] I.Y. Kaplin, E.S. Lokteva, E.V. Golubina, et al., Appl. Surf. Sci. 485 (2019) 432–440.
[14] X. Yang, X. Yu, Q. Yang, et al., Ceram. Int. 43 (2017) 8585–8589.
[15] D. Wang, S. Li, Y. Du, X. Wu, Y. Chen, Catalysts 9 (2019) 352.
[16] S. Liu, J. Ji, Y. Yu, H. Huang, Catal. Sci. Technol. 8 (2018) 4264–4273.
[17] J. Ji, Y. Fang, L. He, H. Huang, Catal. Sci. Technol. 9 (2019) 4036–4046.
[18] F. Buciuman, F. Patcas, R. Craciun, D.R.T. Zahn, PCCP 1 (1999) 185–190.
[19] M. Zhao, J. Deng, J. Liu, et al., ACS Catal. 9 (2019) 7548–7567.
[20] X. Zhang, H. Zhao, Z. Song, et al., Appl. Surf. Sci. 493 (2019) 9–17.
[21] X. Wang, W. Zhao, X. Wu, et al., Appl. Surf. Sci. 426 (2017) 1198–1205.